ACS Catalysis

Research Article

pubs.acs.org/acscatalysis

Improved Thermal Stability and Methane-Oxidation Activity of Pd/Al_2O_3 Catalysts by Atomic Layer Deposition of ZrO_2

Tzia Ming Onn,[†] Shuyi Zhang,[‡,§] Lisandra Arroyo-Ramirez,[†] Yu-Chieh Chung,[†] George W. Graham,[‡] Xiaoqing Pan,[‡,§,∥] and Raymond J. Gorte*[,†]

[†]Department of Chemical and Biomolecular Engineering, University of Pennsylvania, 34th Street, Philadelphia, Pennsylvania 19104, United States

[‡]Department of Materials Science and Engineering, University of Michigan, Ann Arbor, Michigan 48109, United States

[§]Department of Chemical Engineering and Materials Science, University of California−Irvine, Irvine, California 92697, United States

[∥]Department of Physics and Astronomy, University of California−Irvine, Irvine, California 92697, United States

ABSTRACT: The effect of modifying Pd/Al_2O_3 catalysts by atomic layer deposition of 1 nm ZrO_2 films was studied. For deposition on oxidized, PdO/Al_2O_3 catalysts, TEM imaging, EDS mapping, and metal-dispersion measurements confirmed the presence of the thin ZrO_2 over both the Al_2O_3 support and the metal particles. The ZrO_2 films were surprisingly stable, forming a well-crystallized phase only above 1173 K. The ZrO_2 coating over the PdO particles created a semicore−shell-like structure that stabilized the metal against sintering in air at 1073 K. Steady-state, methane oxidation rates on unmodified PdO/Al_2O_3 decreased with increasing catalyst calcination temperature, but rates on the ZrO_2-covered surfaces increased with increasing calcination temperature.

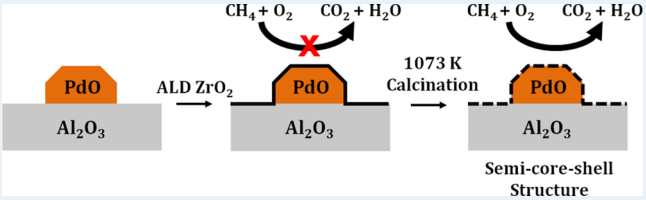

KEYWORDS: *methane oxidation, palladium, thermal stability, improved rates, atomic layer deposition, zirconia*

INTRODUCTION

Stability issues are of great importance in emissions-control catalysis, in which high temperatures and redox cycling can lead to severe deactivation due to sintering of metal catalyst particles.[1] At the same time, there is an increasing need for these catalysts to have low-temperature activity for methane oxidation because of the increasing concern for the global-warming properties of this pollutant.[2] Supported Pd is the material of choice for methane oxidation, and contact between Pd and some oxides, such as ceria,[3,4] is known to promote the reaction.[5−9] However, as noted above, sintering of the Pd particles at high temperatures is a problem.

One method for stabilizing metal catalyst particles involves encapsulating the metal with an oxide. For example, one can produce core−shell structures in which metal nanoparticles are surrounded by a thin shell of oxide.[9] The oxide shell can suppress sintering[10] and in some cases enhance activity for methane oxidation.[9−11] High methane oxidation rates and good thermal stability have been reported for alumina-supported Pd@CeO_2 and Pd@ZrO_2.[9,11] Unfortunately, depending on the method used to produce the core−shell catalyst, synthesis can be complex. In the case of Pd@CeO_2, the catalyst has also been shown to be sensitive to water exposure.[12] Finally, different methods for preparing core−shell catalysts can result in very different catalytic activities, probably because activity depends on the thickness of the oxide shell, which can be difficult to control.[13]

A conceptually related approach to stabilizing metal catalysts involves depositing overlayers of an oxide onto a supported-metal catalyst by atomic layer deposition (ALD).[14] ALD can be used to prepare uniform, atomic-scale, oxide films by repeated reaction of an organometallic precursor with the substrate of interest, followed by oxidation of the surface compound. The thickness of the oxide film is controlled by the number of deposition cycles. This approach has been used to stabilize Co catalysts against leaching for solution-phase reactions by covering the active component with an insoluble oxide, titania.[15] In another case, sintering of Pd/Al_2O_3[16] and Ni/Al_2O_3[17] catalysts was suppressed by depositing a relatively thick alumina coating then heating the overlayers to introduce pores in the ALD overlayers. It is noteworthy that the deposited material in these two examples, along with most of the examples reported in the literature, was an inert oxide similar to the support oxide.

An example that deposited a dissimilar, functionally active oxide involved the use of zirconia overlayers for stabilizing the surface area of perovskite cathodes in solid oxide fuel cells (SOFC).[18] Nanostructured cathodes exhibit better electrode performance because of the increased area for oxygen adsorption on the perovskite component, but nanostructure is difficult to maintain at the high operating temperatures

Received: June 26, 2015
Revised: August 5, 2015
Published: August 24, 2015

DOI: 10.1021/acscatal.5b01348
ACS Catal. 2015, 5, 5696−5701

required by SOFC. Gong, et al. showed that deposition of zirconia overlayers onto the perovskite cathode prevented degradation of electrode performance, presumably by maintaining the initial high surface area of the perovskite. The presence of zirconia did not significantly suppress electrode performance because it is an oxygen ion conductor.

The SOFC electrode example is particularly interesting for emissions-control catalysis because zirconia is already an important component in modern three-way catalysts. The high methane oxidation activity and good thermal stability of $Pd@ZrO_2$ catalysts also suggests that ZrO_2 may act as a promoter for Pd when there is contact between the phases.[11] Therefore, the present study examined the effect of depositing thin films (~1 nm thick) of ZrO_2 onto a PdO/Al_2O_3 catalyst. We demonstrate that the ZrO_2 films create a "semicore−shell"-like structure on the oxidized PdO/Al_2O_3 catalyst, whereas reducing the catalyst prior to ALD of ZrO_2 does not create this structure. Modification of the PdO/Al_2O_3 catalysts by ALD of ZrO_2 reduced the amount of Pd sintering observed after high temperature calcination and stabilized methane oxidation rates.

EXPERIMENTAL METHODS

The Pd/Al_2O_3 catalysts were prepared by incipient wetness onto a γ-Al_2O_3 (Strem Chemicals, Inc.) that had been stabilized by calcining in air at 1173 K for 24 h. The aqueous Pd salt solution was prepared from 0.61 mL of $Pd(NO_3)_2$ (Sigma-Aldrich, 10 wt % in 10 wt % nitric acid) and 0.60 g of citric acid (Sigma-Aldrich) in 10 mL of deionized H_2O. This Pd solution was added dropwise onto 3.0 g of the Al_2O_3, and the resulting mixture was then evaporated at 333 K until the sample was dry. Finally, the catalyst was calcined at 673 K in air for 6 h to remove any organics and nitrates. The above procedure results in a catalyst that is 1 wt % Pd.

ALD of ZrO_2 was performed using a home-built deposition system that has been described in detail in a previous publication.[19] The system consists of two heated chambers, one for the catalyst sample and one for the organometallic precursor, which could be evacuated to $\sim 10^{-3}$ Torr using a mechanical vacuum pump. High-temperature valves separated the two chambers from each other and from both the vacuum pump and a source of water vapor. In a typical experiment, the ZrO_2 precursor, (tetrakis (dimethylamino)-zirconium (TDMZ, Sigma-Aldrich)), was first evacuated then heated to 363 K to produce a TDMZ vapor pressure of ~2 Torr. The TDMZ vapor was then allowed to flow into the evacuated sample chamber, which was held at 453 K, a temperature high enough to avoid condensation of the TDMZ but low enough to prevent chemical vapor deposition. The Pd/Al_2O_3 samples, in either oxidized or reduced form, were exposed to TDMZ vapor for 300 s. In some cases, the samples were evacuated and exposed to TDMZ vapor multiple times to ensure that reaction with the surface was complete. After TDMZ exposure, the samples were again evacuated and exposed to water vapor (~100 Torr) for 300 s. This procedure was repeated as often as desired. Finally, the amount of ZrO_2 deposited on the sample was determined gravimetrically.

The Pd dispersions were determined volumetrically using CO adsorption uptakes at room temperature. In all cases, the samples were pretreated by oxidation in 200 Torr O_2 at 673 K, followed by reduction in 200 Torr H_2 at 423 K. Surface areas were determined from Brunauer−Emmett−Teller (BET) isotherms using N_2 adsorption at 78 K. X-ray diffraction (XRD) patterns were recorded from a Rigaku Smartlab diffractometer equipped with a Cu Kα source. The powdered samples were dispersed thoroughly onto the glass slides using acetone.

Steady-state methane oxidation rates were determined in a 0.25-in. quartz tubular reactor using 100 mg of catalyst. Helium was used as a carrier gas with the partial pressures of CH_4 and O_2 fixed at 3.8 Torr (0.5%) and 38 Torr (5%), respectively. The total flow rate was kept at 110 mL/min. The products were analyzed using a gas chromatograph (SRI8610C) equipped with a Hayesep Q column and a TCD detector. All rates in this study were normalized to the amount of Pd in the catalyst. Differential conversions were maintained in all cases.

Ex situ transmission electron microscopy (TEM) was performed on powder specimens that had been sonicated in methanol and dropped onto carbon support films on copper TEM grids (Ted Pella, Inc.) for TEM examination. In situ TEM was performed on a fresh ALD powder specimen under 150 Torr of O_2 at elevated temperature with an electron transparent gas cell. A detailed description of the gas cell is provided elsewhere.[20] Specimens were examined with a JEOL 3100R05 electron microscope with double spherical aberration correctors operated at 300 kV in scanning mode. The microscope is equipped with a horizontal ultrathin Window JEOL SDD X-ray detector capable of detecting elements with $Z > 5$ and Gatan no. 965 Quantum imaging filter (GIF) for electron energy loss spectroscopy.

RESULTS

Characterization of ZrO_2 Film Growth. To determine the growth rate for ZrO_2 films on PdO/Al_2O_3, the weight of the catalyst was measured as a function of the number of TDMZ−H_2O cycles, with the results shown in Figure 1. It is important

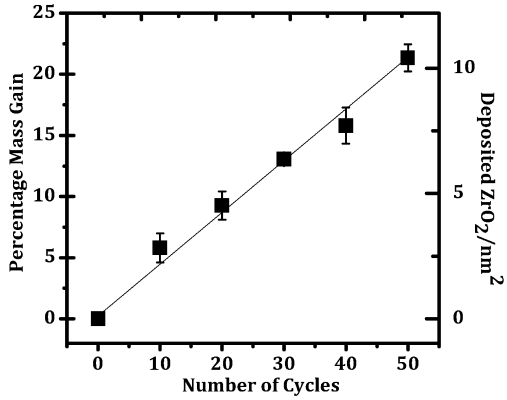

Figure 1. Mass change as a function of the number of ALD cycles on a PdO/Al_2O_3 catalyst that had an initial surface area of 100 m^2/g.

to note that the Al_2O_3 support used in this study had been calcined to 1173 K for stabilization and had a surface area of only 100 m^2/g. Previous studies of an essentially identical Al_2O_3 treated in this way showed that this treatment gave rise to a material with an average pore diameter of 20 nm.[9] Because this is much greater than the size of the TDMZ precursor, the surface can be considered "flat" with respect to deposition. For the data in Figure 1, the catalyst was removed from the ALD system after every 10th TDMZ−H_2O cycle and then calcined in flowing air at 673 K to ensure complete removal of all carbon. The data demonstrate that the mass increased linearly with the number cycles in this coverage range, increasing by 21% after 50 cycles. Assuming that the ZrO_2 film deposits

DOI: 10.1021/acscatal.5b01348
ACS Catal. 2015, 5, 5696−5701

uniformly and with a density equal to that of tetragonal ZrO_2, the film growth was 0.02 nm/cycle (10 Zr atoms/nm^2 after 50 cycles). This deposition rate is low partly because of the large size of the TDMZ precursor, but the growth rate is higher than the value reported for CeO_2 films deposited on doped $LaFeO_3$ using a tetrakis(2,2,6,6-tetramethyl-3,5-heptanedionato)cerium precursor.[19] Finally, the growth curve here was measured with Pd left in the oxidized state prior to ALD−ZrO_2, but similar ZrO_2 loadings were obtained after 50 cycles when ZrO_2 was grown on a reduced sample.

The samples were also characterized using BET. As shown in Table 1, the surface area decreased from 100 to 66 m^2/g after

Table 1. BET Surface Areas of Samples Used in This Study

Support	BET Surface Area (m^2/g)	
Al_2O_3	100	
Calcination Temp	PdO/Al_2O_3	$50ZrO_2$−PdO/Al_2O_3
773 K	100	66
973 K	100	66
1073 K	100	70

50 deposition cycles. In addition, the surface area was essentially unaffected by increasing the calcination temperature from 773 to 1073 K. The addition of 0.21 g of ZrO_2/g catalyst would be expected to decrease the specific surface area from 100 to 83 m^2/g simply as a result of the change in mass of the sample. An additional loss in specific surface area would come from changing the average pore size of the Al_2O_3 from 20 to 18 nm because of the 1 nm ZrO_2 film, decreasing the expected surface area 10% so that the specific surface area would be 74 m^2/g. Because smaller pores have a disproportionally larger impact on surface area of a material with a distribution of pore sizes, coating of those smaller pores could explain the decrease to 66 m^2/g.

Scanning transmission electron microscopy (STEM) and EDS mapping also offered insights into the surface coverage of ZrO_2 on PdO/Al_2O_3. A comparison of the ALD-coated and uncoated sample after 773 and 1073 K calcination is shown in Figure 2a−d. The PdO particles are of comparable sizes, ∼5 nm in diameter, in both the ZrO_2-coated (Figure 2a) and uncoated (Figure 2c) samples after 773 K calcination; however, the sizes of PdO particles with the ZrO_2 protective layer remained unaffected after heating to 1073 K in air (Figure 2b). In contrast, the size of the particles almost doubled in the uncoated PdO/Al_2O_3 sample after the same treatment. This observation is consistent with previous TEM analysis after ALD of a metal oxide was carried out.[15] In addition, sintering or signs of aggregation were frequently observed by the TEM for PdO/Al_2O_3 calcined at 1073 K, but these events were rarely observed with $50ZrO_2$−PdO/Al_2O_3. High angle annular dark field (HAADF) imaging, in which ZrO_2 appears brighter than Al_2O_3 because of the atomic number difference between Zr and Al, allows the ZrO_2 surface layer to be distinguished from Al_2O_3, as shown in Figure 2e,f. Here, the Al_2O_3 support appears to be covered by a uniform ZrO_2 surface layer with thickness of ∼1 nm in the fresh sample without calcination. EDS elemental maps, including Pd, Zr, and Al, on the same sample, shown in Figure 3, confirm that the brightness variation on Al_2O_3 is due to the presence of Zr, and they further confirm that the PdO particles are fully covered by the ZrO_2 layer as a result of the coincidence of Zr and Pd in the spectra. It should be noted that Zr species, when observed under the TEM, appeared in three

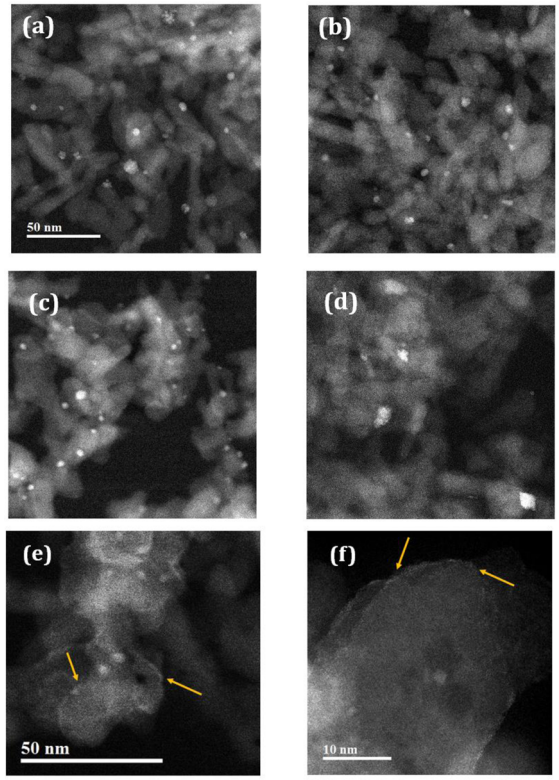

Figure 2. STEM results for PdO/Al_2O_3 and $50ZrO_2$−PdO/Al_2O_3 catalysts after various pretreatments: (a) $50ZrO_2$−PdO/Al_2O_3 calcined at 773 K; (b) $50ZrO_2$−PdO/Al_2O_3 calcined at 1073 K; (c) PdO/Al_2O_3 calcined at 773 K; (d) PdO/Al_2O_3 calcined at 1073 K; (e, f) $50ZrO_2$−PdO/Al_2O_3 uncalcined (fresh). Arrows in parts e and f indicate regions of high contrast due to the ZrO_2 overlayer.

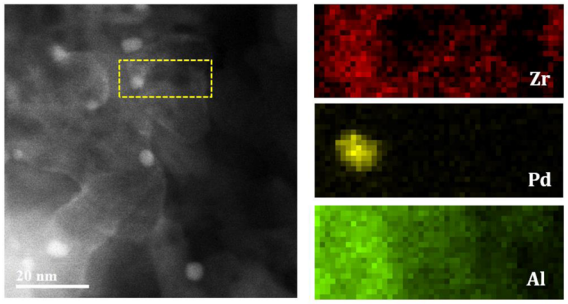

Figure 3. STEM results for uncalcined (fresh) $50ZrO_2$−PdO/Al_2O_3 catalysts with EDS mapping of Al, Zr, and Pd.

different forms: a thin ZrO_2 layer on the Al_2O_3 surface, a thin layer around the PdO particle, and sometimes small chunks.

XRD patterns from Figure 4 confirmed that the ZrO_2 layers were initially amorphous, not crystalline. We observe that, upon heating to 773 and 1073 K (Figure 4b,c, respectively), there were no observable features due to crystalline ZrO_2 from the ALD ZrO_2 samples. However, when the sample was heated to 1173 K in air (Figure 4d), we observed small peaks near 30 and 50 degrees 2θ aligned with the characteristic diffraction patterns of a tetragonal ZrO_2 phase. The corresponding size of ZrO_2 crystallites was calculated to be around 5 nm on the basis of the width of the peak at around 30° at half-maximum from the Scherrer equation. This result is consistent with the formation of a thin ZrO_2 layer that forms particles upon high temperature calcination. In situ TEM observations revealed that the thin

DOI: 10.1021/acscatal.5b01348
ACS Catal. 2015, 5, 5696−5701

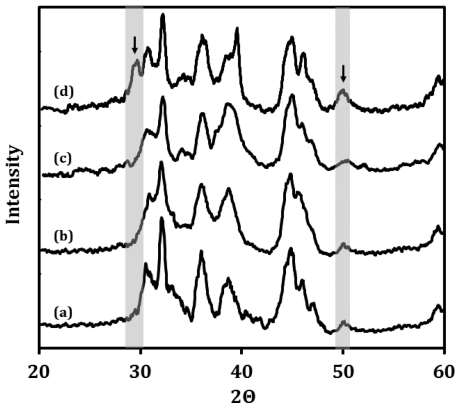

Figure 4. XRD patterns of the ALD-coated, $50ZrO_2$–PdO/Al_2O_3 sample after calcination to various temperatures: (a) as deposited; (b) 773; (c) 1073; and (d) 1173 K. Characteristic peaks for tetragonal ZrO_2 are marked by the gray lines.

ZrO_2 layer on the Al_2O_3 surface actually begins to migrate and form into nanoparticles at much lower temperature, 773 K, as shown in Figure 5. Here, since the area imaged clearly contains

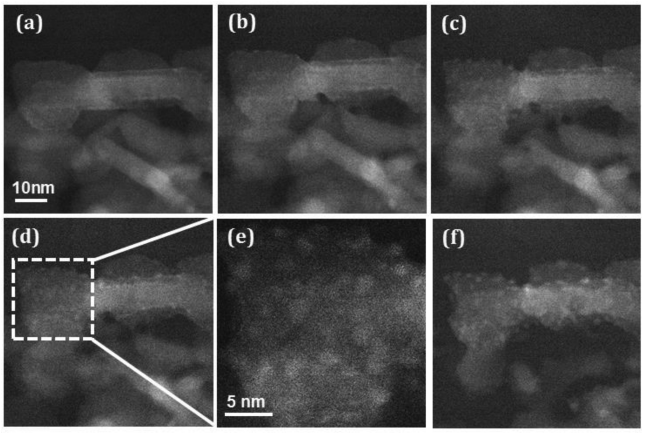

Figure 5. Sequential STEM images of uncalcined (fresh) $50ZrO_2$–PdO/Al_2O_3 catalysts obtained in situ under 150 Torr O_2 in the TEM gas cell at a temperatures of (a) 573; (b, c) 773 for 0 and 3 min respectively; (d, e) 873; and (f) 973 K.

no PdO particles initially, the particles that are observed to form with increasing time and temperature are certainly zirconia. These observations provide direct evidence for the effect of calcination temperature on catalytic activity, presented below. Finally, we also note that the ZrO_2 surface layer was not observed in many areas examined by TEM, presumably because it was too thin to detect by either HAADF imaging or EDS.

Methane Oxidation Rates. Methane oxidation was used to probe the effect of ZrO_2 films on the catalytic performance of Pd/Al_2O_3 catalysts, prepared by ALD on both oxidized and reduced catalysts. Steady state rate measurements were carried out under differential conditions in 0.5% CH_4 and 5.0% O_2 with helium as the carrier gas. Figure 6a is an Arrhenius plot showing rates for the unmodified Pd/Al_2O_3 sample following calcination at 773, 973, and 1073 K. The activation energies are roughly the same, 90 kJ/mol, but the rates decrease noticeably as the calcination temperature increased. The catalyst calcined at 773 K exhibited rates that were approximately five times higher than the catalyst calcined at 1073 K. This decrease in rates is at least

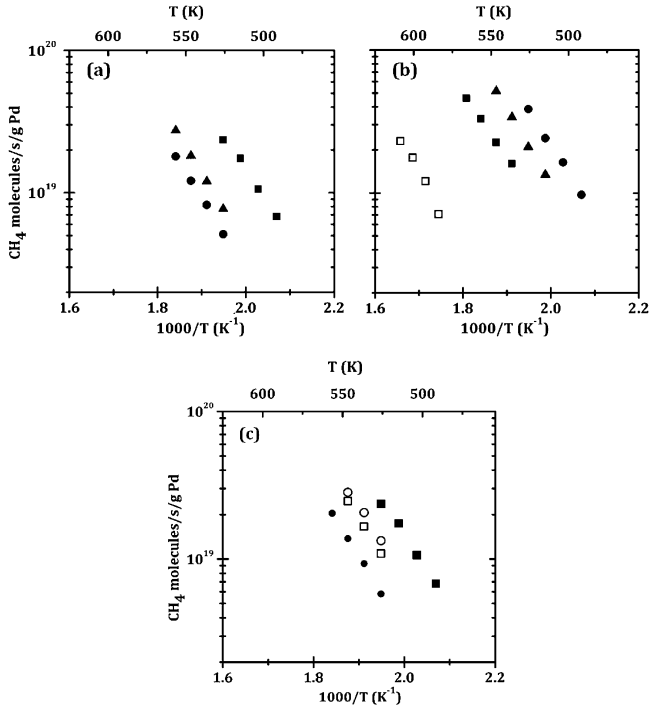

Figure 6. Steady-state, differential reaction rates for methane oxidation in 0.5% CH_4 and 5% O_2. (a) Rates on PdO/Al_2O_3 after calcination to the following temperatures: (■) 773, (▲) 973, and (●) 1073 K. (b) Rates on $50ZrO_2$–PdO/Al_2O_3 after calcination to the following temperatures: (□) uncalcined, (■) 773, (▲) 973, and (●) 1073 K. (c) Rates on $50ZrO_2$–Pd/Al_2O_3, in which ZrO_2 was deposited on the reduced catalysts by ALD, after calcination at (□) 773 and (○) – 1073 K. Data for PdO/Al_2O_3 calcined at (■) 773 and (●) 1073 K are shown for comparison.

partially explained by the increase in Pd particle size with calcination temperature observed in the TEM measurements discussed earlier. Dispersion measurements, reported in Table 2, also indicate a decrease in the available Pd surface area,

Table 2. Pd Metal Dispersions of Samples Used in This Study

	dispersion (%)		
calcination temp	PdO/Al_2O_3	$50ZrO_2$–PdO/Al_2O_3	$50ZrO_2$–Pd/Al_2O_3
773 K	32.9	10.6	18.5
973 K	29.8	10.8	
1073 K	24.2	13.2	18.6

decreasing from 33% to 24% after heating the catalyst from 773 to 1073 K. Clearly, the decrease in rates was significantly greater than the decrease in dispersion, implying that other factors must also be involved. Methane oxidation rates have been reported to depend on Pd crystallite size[21−23] and the presence of support hydroxyls on Al_2O_3,[24,25] but increased calcination temperature appears to influence rates by changing more than just the metal surface area.[19,22,26]

Rates for the sample prepared with 50 ALD cycles of ZrO_2 deposited onto the oxidized PdO/Al_2O_3 catalyst are shown in Figure 6b. The catalyst calcined at 773 K, designated $50ZrO_2$–$PdO/Al_2O_3(773)$, showed very low rates. Whereas the unmodified Pd/Al_2O_3 catalyst calcined at 773 K exhibited a rate of 10^{19} $CH_4/(s{\cdot}g\ Pd)$ at a temperature of 500 K, the $50ZrO_2$–$PdO/Al_2O_3(773)$ sample was able to achieve this rate

DOI: 10.1021/acscatal.5b01348
ACS Catal. 2015, 5, 5696−5701

at 530 K only through extrapolation; however, the activity of this catalyst increased dramatically with increasing calcination temperature. After heating to 1073 K, the temperature at which the rate was 10^{19} $CH_4/(s{\cdot}g\ Pd)$ was 485 K, indicating that $50ZrO_2{-}PdO/Al_2O_3(1073)$ catalyst was more active than even fresh Pd/Al_2O_3. Because the STEM results indicated that the Pd particles were covered by the ZrO_2 film following ALD, it is likely the increased rates are due to breaking up of that ZrO_2 film. Again, changes in the rates were not reflected by changes in the dispersions measured by CO adsorption, shown in Table 2. The relatively high activity of the $50ZrO_2{-}PdO/Al_2O_3$ (1073) catalyst must be due in part to interactions with ZrO_2.

Methane oxidation rates for a catalyst prepared by 50 ALD cycles of ZrO_2 onto reduced Pd/Al_2O_3 are shown in Figure 6c. Rates for the unmodified Pd/Al_2O_3 after calcination at 773 and 1073 K are shown for comparison. Interestingly, rates on the $50ZrO_2{-}Pd/Al_2O_3$ samples were the same when calcined at either 773 or 1073 K. Rates were somewhat lower than for the unmodified Pd/Al_2O_3 calcined at 773 K but were stable. The measured dispersions on this catalyst were higher than that measured on $50ZrO_2{-}PdO/Al_2O_3$ catalysts and did not change with calcination temperature. We suggest that, in this case, the ZrO_2 film did not grow on the metallic Pd, so there was no need to "break up" the oxide film. However, the presence of the ZrO_2 film on the Al_2O_3 does appear to thermally stabilize the Pd particles.

DISCUSSION

ALD is an intriguing method for promoting supported-metal catalysts.[14] The structure of the oxide films prepared by ALD is clearly very different from what could be achieved by adding an oxide promoter using infiltration or coprecipitation methods. Although most other methods of adding oxides will tend to form oxide particles or are limited to forming a single oxide monolayer, ALD allows formation of thin films of varying thickness. The observation from this work that ZrO_2 films could grow on PdO but not on Pd also suggests that it may be possible to deposit promoters over only selected parts of the catalyst. The present study did not explore compositional changes, but ALD clearly allows deposition of a wide range of materials.

It is interesting to notice that the properties of the Pd/Al_2O_3 catalysts with 1 nm ZrO_2 overlayers prepared by ALD have many similarities to $Pd@ZrO_2/Al_2O_3$, core−shell catalysts that have been described in a previous publication.[11] In that case, the $Pd@ZrO_2$ particles were prepared in solution to have a ∼ 2 nm ZrO_2 shell covering Pd nanoparticles, then adsorbed onto functionalized Al_2O_3. In both cases, the ZrO_2 films were found to stabilize the Pd particles against sintering at high temperatures. The ZrO_2-covered Pd catalysts also exhibited enhanced activity for methane oxidation.

The reason for the enhanced methane oxidation rates on the zirconia-promoted catalysts is uncertain. The literature shows that methane oxidation on Pd is a complex reaction that likely involves C−H activation on sites in the vicinity of both metallic Pd and PdO.[27] Although there is strong evidence that C−H bond activation is structure-sensitive in Pd, there is controversy over whether particle size influences reaction rates, with some reporting that larger particles exhibit higher specific rates[21,22] and others reporting that rates are strictly proportional to the surface area of the Pd or PdO.[28] There is agreement that PdO must be present in the active phase; but the stability of PdO, along with the reaction rate for methane, can be influenced by the oxide support.[24−26] In past work on $Pd@ZrO_2$ core−shell catalysts, evidence was presented that the ZrO_2 in contact with the Pd is reducible and that this reducibility is somehow responsible for stabilizing PdO and enhancing reaction rates.[11]

Another interesting observation from the present study is that the ZrO_2 films deposited by ALD were XRD-amorphous to high temperatures. There was some evidence from TEM for changes in the film at 773 K, but the crystallization is clearly suppressed. One would normally expect that thin films would be highly unstable and that the zirconia would try to minimize its free energy by forming crystalline particles. Interactions with the alumina must somehow suppress this crystallization. One would expect these effects to be strongly dependent on the thickness of the zirconia film. How important the crystalline structure for zirconia might be is uncertain. With ceria, it is well established that reducibility is affected by the crystalline structure.[29]

The mechanism by which the zirconia films stabilize Pd sintering is not completely understood. Sintering is most severe when PdO decomposes to form Pd, which normally occurs above 1073 K. Although the zirconia film may simply stabilize the particles through physically covering the particles, it is also possible that the proximity between the Pd and zirconia could stabilize the PdO phase, as has been observed in $Pd@ZrO_2$ core−shell catalysts.[11] Although there have been many studies of catalyst preparation by ALD, we believe this area of work is still in its infancy. Even considering only applications in which ALD is used to add promoters to metal catalysts, there are many variables that have yet to be explored, including composition of the deposits and thickness of the films. The present work provides an example to further demonstrate the promise of this approach.

CONCLUSION

Modification of PdO/Al_2O_3 catalysts by ALD deposition of 1 nm ZrO_2 films is shown to result in catalysts with a semicore−shell structure. The ZrO_2 films stabilize Pd against sintering at high temperatures and enhance the methane oxidation activity of these catalysts following high-temperature calcination.

AUTHOR INFORMATION

Corresponding Author

*E-mail: gorte@seas.upenn.edu.

Notes

The authors declare no competing financial interest.

ACKNOWLEDGMENTS

T.M.Z. and R.J.G. are grateful to the Department of Energy, Office of Basic Energy Sciences, Chemical Sciences, Geosciences and Biosciences Division, Grant No. DE-FG02-13ER16380 for support of this work. S.Z., G.G., and X.P. are grateful to the National Science Foundation, Grant Nos. CBET-1159240 and DMR-0723032 for support of this work.

REFERENCES

(1) McCarty, J. G.; Malukhin, G.; Poojary, D. M.; Datye, A. K.; Xu, Q. *J. Phys. Chem. B* **2005**, *109*, 2387−2391.
(2) Farrauto, R. J. *Science* **2012**, *337*, 659−660.
(3) Colussi, S.; Gayen, A.; Farnesi Camellone, M.; Boaro, M.; Llorca, J.; Fabris, S.; Trovarelli, A. *Angew. Chem., Int. Ed.* **2009**, *48*, 8481.
(4) Cargnello, M.; Jaen, J. J. D.; Garrido, J. C. H.; Bakhmutsky, K.; Montini, T.; Gamez, J. J. C.; Gorte, R. J.; Fornasiero, P. *Science* **2012**, *337*, 713−717.

DOI: 10.1021/acscatal.5b01348
ACS Catal. 2015, 5, 5696−5701

(5) Forzatti, P.; Groppi, G. *Catal. Today* **1999**, *54*, 165−180.
(6) Ciuparu, D.; Lyubovsky, M. R.; Altman, E.; Pfefferle, L. D.; Datye, A. *Catal. Rev.: Sci. Eng.* **2002**, *44*, 593−649.
(7) Kucharczyk, B.; Tylus, W.; Kepiński, L. *Appl. Catal., B* **2004**, *49*, 27−37.
(8) Gelin, P.; Primet, M. *Appl. Catal., B* **2002**, *39*, 1−37.
(9) Farrauto, R. J.; Hobson, M. C.; Kennelly, T.; Waterman, E. M. *Appl. Catal., A* **1992**, *81*, 227−237.
(10) Adijanto, L.; Bennett, D.; Chen, C.; Yu, A. S.; Cargnello, M.; Fornasiero, P.; Gorte, R. J.; Vohs, J. M. *Nano Lett.* **2013**, *13*, 2252−2257.
(11) Chen, C.; Yeh, Y.-H.; Cargnello, M.; Murray, C. B.; Fornasiero, P.; Gorte, R. J. *ACS Catal.* **2014**, *4*, 3902−09.
(12) Monai, M.; Montini, T.; Chen, C.; Fonda, E.; Gorte, R. J.; Fornasiero, P. *ChemCatChem* **2015**, *7*, 2038−2046.
(13) Cargnello, M.; Fornasiero, P.; Gorte, R. J. *Catal. Lett.* **2012**, *142*, 1043−48.
(14) O'Neill, B. J.; Jackson, D. H. K.; Lee, J.; Canlas, C.; Stair, P. C.; Marshall, C. L.; Elam, J. W.; Kuech, T. F.; Dumesic, J. A.; Huber, G. W. *ACS Catal.* **2015**, *5*, 1804−1825.
(15) O'Neill, B. J.; Jackson, D. H. K.; Crisci, A. J.; Farberow, C. A.; Shi, F.; Alba-Rubio, A. C.; Lu, J.; Dietrich, P. J.; Gu, X.; Marshall, C. L.; Stair, P. C.; Elam, J. W.; Miller, J. T.; Ribeiro, F. H.; Voyles, P. M.; Greeley, J.; Mavrikakis, M.; Scott, S. L.; Kuech, T. F.; Dumesic, J. A. *Angew. Chem.* **2013**, *125*, 14053−14057.
(16) Lu, J.; Fu, B.; Kung, M. C.; Xiao, G.; Elam, J. W.; Kung, H. H.; Stair, P. C. *Science* **2012**, *335*, 1205−1208.
(17) Gould, T. D.; Izar, A.; Weimer, A. W.; Falconer, J. L.; Medlin, J. W. *ACS Catal.* **2014**, *4*, 2714−2717.
(18) Gong, Y.; Palacio, D.; Song, X.; Patel, R. L.; Liang, X.; Zhao, X.; Goodenough, J. B.; Huang, K. *Nano Lett.* **2013**, *13*, 4340−4345.
(19) Yu, A. S.; Küngas, R.; Vohs, J. M.; Gorte, R. J. *J. Electrochem. Soc.* **2013**, *160*, F1225−F1231.
(20) Zhang, S.; Cargnello, M.; Cai, W.; Murray, C. B.; Graham, G. W.; Pan, X. *manuscript in preparation*.
(21) Briot, P.; Primet, M. *Appl. Catal.* **1991**, *68*, 301.
(22) Stakheev, A. Y.; Batkin, A. M.; Teleguina, N. S.; Bragina, G. O.; Zaikovsky, V. I.; Prosvirin, I. P.; Khudorozhkov, A. K.; Bukhtiyarov, V. I. *Top. Catal.* **2013**, *56*, 306.
(23) Muller, C. A.; Maciejewski, M.; Koeppel, R. A.; Baiker, A. *Catal. Today* **1999**, *47*, 245.
(24) Schwartz, W. R.; Ciuparu, D.; Pfefferle, L. D. *J. Phys. Chem. C* **2012**, *116*, 8587−8593.
(25) Ciuparu, D.; Perkins, E.; Pfefferle, L. *Appl. Catal., A* **2004**, *263*, 145−153.
(26) Farrauto, R. J.; Lampert, J. K.; Hobson, M. C.; Waterman, E. M. *Appl. Catal., B* **1995**, *6*, 263−270.
(27) Fujimoto, K. I.; Ribeiro, F. H.; Avalos-Borja, M.; Iglesia, E. *J. Catal.* **1998**, *179*, 431.
(28) Zhu, G.; Han, Y.; Zemlyanov, D. Y.; Ribeiro, F. H. J. *J. Am. Chem. Soc.* **2004**, *126*, 9896.
(29) Gorte, R. J. *AIChE J.* **2010**, *56*, 1126−1135.

DOI: 10.1021/acscatal.5b01348
ACS Catal. 2015, 5, 5696−5701